Chapter - 5

Synthesis and Photoluminescence Studies of undoped and Europium doped Barium Cerium Niobate Oxide

5.1 Introduction

The $A_2BB'O_6$ type double pervoskite structure has a vital interest to materials scientists and solid-state chemists. This attention is often due to their potential application as substrates for high-Tc superconductors, especially for applications in the microwave region [1 – 5]. Double pervoskite-type oxides are suitable for such purposes due to their outstanding dielectric properties, including a low dielectric loss, low chemical reactivity, and their compatibility with some of the most regularly used superconductors, particularly as a result of owning an appropriate thermal expansion co-efficient. They are concern as they give a material where the magnetic properties of lanthanides studied in a relatively significant octahedral environment [6 – 10] and have been recently reviewed for their potential use as luminescent materials [11].

Pervoskite is a new derivative of a close-packed structure in which the oxygen arranged in a cubic close-packed organization except one oxygen ion is missing in every second layer, leaving a large volume void in the center. The strength of pervoskite to accommodate large cations of rare earth elements makes it novel among the close-packed oxides. If the 12-coordinated cation is smaller compared to the oxide ion, the tilting of octahedra changes the pervoskite structure [12]. The modified structure produced after tilting could be tetragonal, orthorhombic, monoclinic, or sometimes without any center of symmetry. Non-centric pervoskites display piezoelectricity or ferroelectricity, and synthetic pervoskites used as electronic sensors. The structure of the newly discovered high-temperature superconductor shows resemblance with pervoskite structure [13].

Around 90% of the natural metallic elements of the periodic table are known to be stable in a pervoskite-type oxide structure. Pervoskites have sub-metallic to metallic luster, colorless streak, cube-like structure along with imperfect cleavage, and brittle tenacity. Pervoskite structured ceramic materials with general chemical formula ABO_3 are value-added materials used for several applications such as capacitors [14], non-volatile memories [15, 16], actuators and sensors [17 – 19], piezoelectric [20], ultrasonic and underwater devices [21], high-temperature heating applications [13], frequency filters for wireless communications [22], etc. Pervoskites can be prepared in various forms like nanocrystalline, bulk, thin films, and rods depending on their applications [23].

It's well known that the complex oxides having pervoskite-type structure usually show functional properties [24, 25]. Among them, the researcher paid attention to the Ba_2LnNbO_6 (Ln = lanthanide elements) compounds. Ba_2LnNbO_6 type pervoskite compound was first synthesized by Brixner [24] and found to have a cubic pervoskite-type structure for all except for Ln = La, which is tetragonally distorted structure, and some of them have ferroelectric properties. Later, Filip'ev et al. [26] reported that the structure of Ln = La had a rhombohedral distorted structure. Anderson et al. [27], however, point out that the crystal system of $A_2BB'O_6$ double pervoskites is cubic, orthorhombic, or monoclinic because the B/B'-cation arrangement is limited to be a random type, a rock salt type, or a layered type. When the B/B'- cation arrangement is a rock salt type, the crystal system should be either a cubic one ($Fm\bar{3}m$) [28, 29]or a monoclinic one ($P2_1/n$) [30, 31], for random type arrangement, the crystal system should be either a cubic one ($Pm\bar{3}m$) [29, 32] or a orthorhombic one (Pbnm) [30, 33] and for layered type, the crystal system should be monoclinic one ($P2_1/n$) [34].

Practically all kinds of optical centres were studied in the pervoskite structure for various doped concentrations. The studies of optical properties of pervoskite systems have contributed considerably to the development of many optical materials like LASER materials, solar energy conversion and many more [35, 36].

Although, the permittivity measurement at microwave frequencies of many niobate have been performed by other researchers [37]. There is no reported data were found on photoluminescence properties of rare earth doped Ba_2CeNbO_6 during the literature survey. Our group report the photoluminescence studies of Ba_2CeNbO_6 doped with Eu (III).

5.2 Synthesis and Characterization

5.2.1 Synthesis

Eu(III) doped Ba_2CeNbO_6 phosphor had been synthesized by the combustion method. Starting chemicals used for this objective are $Ba(NO_3)_2$, $Ce(NO_3)_3.6H_2O$, Nb_2O_5, Eu_2O_3, and urea as flux. These chemicals were intimately mixed in the stoichiometric ratio corresponding to the nominal composition of Eu(III) doped Ba_2CeNbO_6 and transferred into alumina crucible. Then, this mixture was fired at 800ºC in a muffle furnace for 3 hours and then allowed it naturally cool to room

temperature. The synthesized material ground using mortar – pastel was obtained in powder form owning white color.

5.2.2 Characterization

XRD measurements of undoped and Eu(III) doped Ba2CeNbO6, were done on D8 Bruker advance X-Ray Diffractometer with the Cu Kα radiation with 8.05keV energy, and 1.5406 Å wavelength (λ) at room temperature by step scanning in an angle range of $20° \leq 2\theta \leq 70°$ with increments of 0.02º. FTIR spectra of phosphors were, recorded using Jasco FTIR- 4100, spectrophotometer (Japan) by mixing phosphor with KBr in mortar - pestle in a ratio of 1:10. The PL of the samples examined using a Shimadzu spectrofluorophotometer (RF-5301 PC) at room temperature with a xenon lamp as an excitation source.

5.3 Results and Discussion

5.3.1 X-Ray Diffraction

Figure 5.1 exhibits room-temperature powder X-ray diffraction pattern of undoped, and Eu(III) doped Ba_2CeNbO_6. The recorded patterns present sharp and well-defined peaks, indicating that the as prepared materials have a highly crystalline nature. There is a good agreement between the observed and calculated interplanar spacing (d-values) that suggest that the compound has a monoclinic phase with a $P2_1/n$ (#14) space group. The relative coordinates and occupancy of each site for Ba_2CeNbO_6 are shown in Table 5.1. The values for the bond distances of cations (relative to the oxygen anion) and occupancy were obtained from the Rietveld refinement. These are shown in Table 5.2. These diffraction lines are consistent and confirm the formation of a double pervoskite structure for all studied samples. The average crystallite sizes were estimated by the Scherrer's equation using the full width at half maximum (FWHM) of all intense peak. The average crystallite size calculated using the Debye-Scherrer formula given in the literature [38] which is given as equation (5.1),

$$D = \frac{k.\lambda}{\beta.Cos\theta} \qquad \text{----------} \qquad (5.1)$$

Where, D is the average crystallite size, k is the constant equal to 0.94, λ is the wavelength of the X-rays equal to 0.1542 nm, θ is the Bragg angle and β is FWHM. All

the reflection peaks of the X-ray profile indexed and lattice parameters are determined with the help of a standard computer program Powder-X.

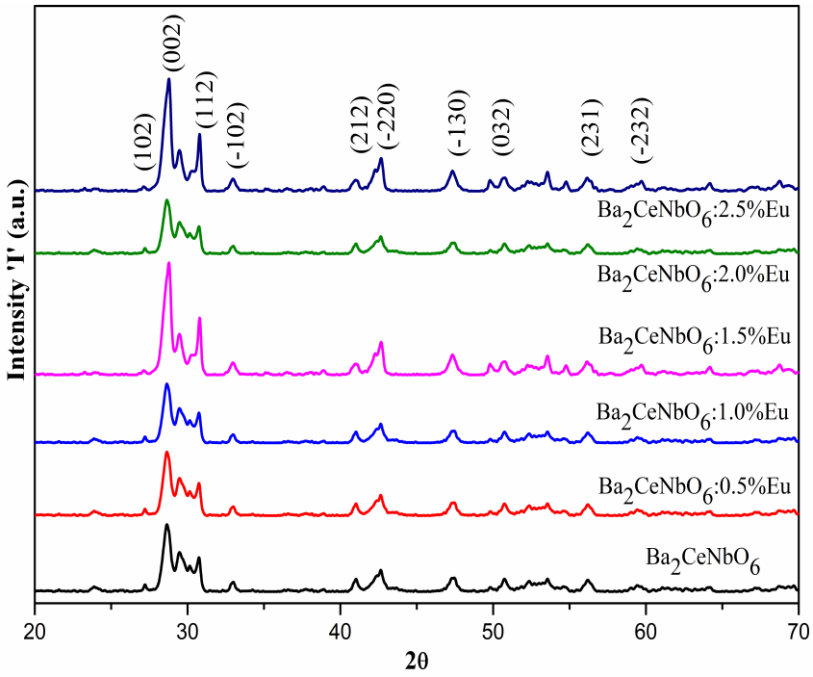

Figure 5.1 X-ray diffraction pattern of undoped and Eu(III) doped Ba_2CeNbO_6.

Atom	Site	*X*	*y*	*Z*
Ba	4e	0.5000	0.5000	0.2395
Ce	2c	0.0000	0.5000	0.0000
Nb	2d	0.5000	0.0000	0.0000
O	4e	0.2692	0.2167	0.0000
O	4e	0.2692	0.7833	0.0000
O	4e	0.5000	0.0000	0.2255

Table 5.1 Structural parameters of Ba_2CeNbO_6 found by Rietveld analysis of XRD data.

Cation	Anion & Multi.	Distance (Å)	Occupancy
Ce (2c)	O (4e) X 2	2.4475	1.00
Ce (2c)	O (4e) X 2	2.4475	1.00
Ce (2c)	O (4e) X 2	2.4075	1.00
Nb (2d)	O (4e) X 2	1.9824	1.00
Nb (2d)	O (4e) X 2	1.9824	1.00
Nb (2d)	O (4e) X 2	1.9785	1.00
Ba (4e)	O (4e) X 1	3.1067	1.00
Ba (4e)	O (4e) X 1	3.1471	1.00
Ba (4e)	O (4e) X 1	3.1067	1.00
Ba (4e)	O (4e) X 1	3.1471	1.00
Ba (4e)	O (4e) X 1	3.1067	1.00
Ba (4e)	O (4e) X 1	3.1471	1.00
Ba (4e)	O (4e) X 1	3.1067	1.00
Ba (4e)	O (4e) X 1	3.1471	1.00
Ba (4e)	O (4e) X 1	3.1461	1.00
Ba (4e)	O (4e) X 1	3.1461	1.00
Ba (4e)	O (4e) X 1	3.1636	1.00
Ba (4e)	O (4e) X 1	3.1636	1.00

Table 5.2 Inter-atomic distance and occupancy calculated through Rietveld refinement of experimental data.

All the reflection peaks of the X-ray profile indexed, and lattice parameters are determined with the help of a standard computer program Powder-X. In double pervoskite oxide, the study of distortion from the ideal cubic pervoskite structure is clear as the Ba_2CeNbO_6 complex pervoskite has the general formula $A_2BB'O_6$. The tolerance factor T_f [39] of the sample is calculated by using equation (5.2),

$$T_f = \frac{R_{Ba}+R_O}{\sqrt{2}\left(\frac{R_{Ce}+R_{Nb}}{2}+R_O\right)} \quad \text{---------- (5.2)}$$

Where, R_{Ba}, R_{Ce}, R_{Nb} and R_O are the ionic radii of Ba, Ce, Nb and O respectively [40]. By the geometry of crystal, the ideal cubic structure should have $T_f = 1$, whereas it will be monoclinic structure for values of $T_f < 1$ and it following the SPuDs prediction [41]**.** The value of tolerance factor for Ba_2CeNbO_6 was found to be approximately 0.9505, which suggests that sample under study has the monoclinic structure.

Williomson – Hall Plot

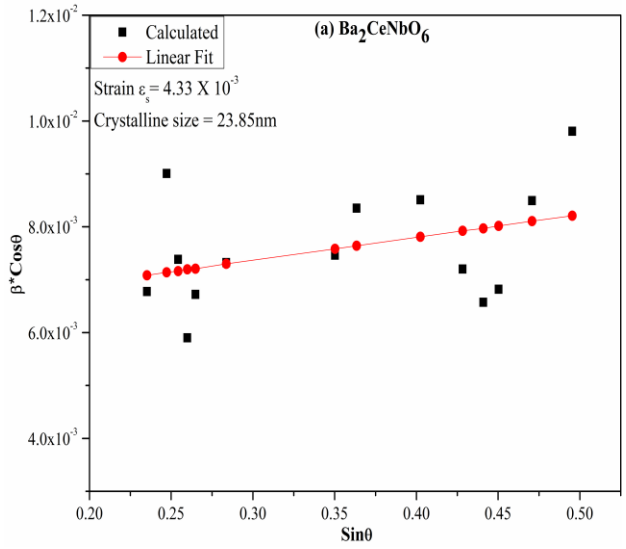

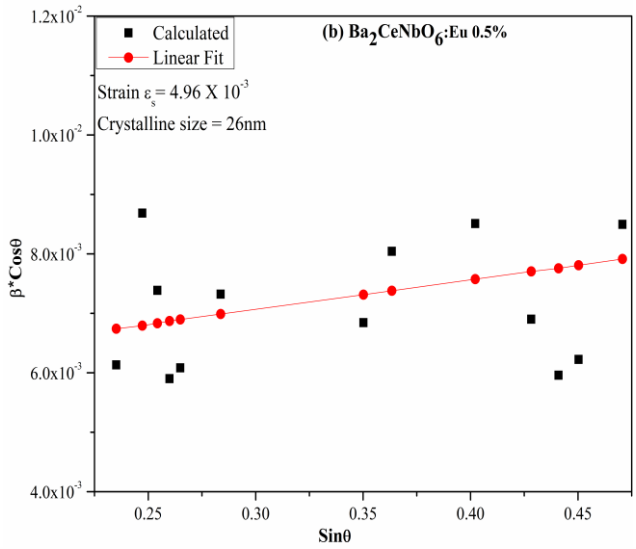

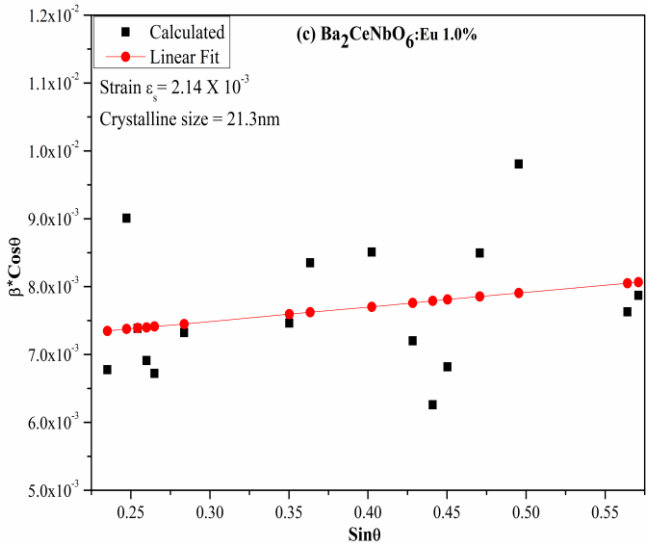

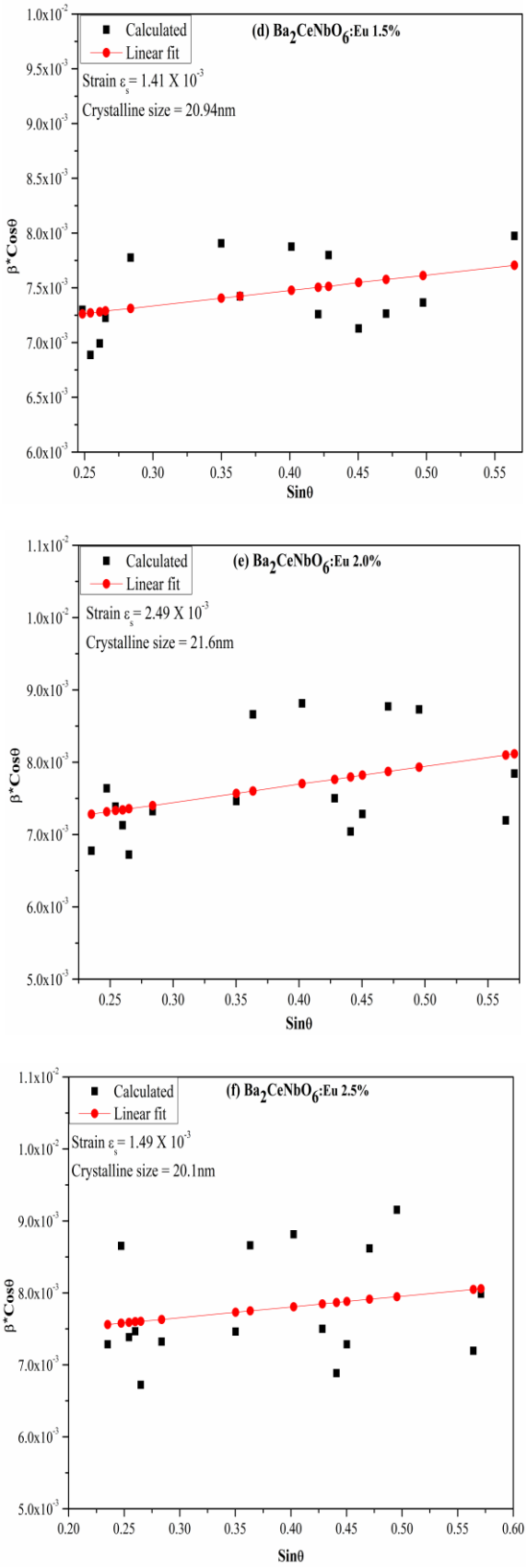

Figure 5.2 (a-f) Williomson-Hall plot of undoped and Eu(III) doped Ba_2CeNbO_6.

Figure 5.2 (a-f) shows W-H plot of undoped and Eu (III) doped Ba_2CeNbO_6. The broadening effect of XRD peaks reflects the nanocrystalline nature of the resulting Eu(III) doped Ba_2CeNbO_6 samples. Since the effective XRD peak broadening can caused by lattice strain and small crystallite size, these two effects have to be distinguished. This can be calculated by plotting β cosθ versus sinθ in the following relation (equation 5.3) (Williamson–Hall plot) [38],

$$\beta_{hkl} * cos\theta_{hkl} = \left(\frac{k\lambda}{D}\right) + \varepsilon * sin\theta_{hkl} \text{ ---------- (5.3)}$$

The crystallite size and strain of Eu(III) doped Ba_2CeNbO_6 estimated from the intercept and slope are listed in Table 5.3.

Sample		Ba_2CeNbO_6	Ba_2CeNbO_6: Eu^{3+} (0.5%)	Ba_2CeNbO_6: Eu^{3+} (1.0%)	Ba_2CeNbO_6: Eu^{3+} (1.5%)	Ba_2CeNbO_6: Eu^{3+} (2.0%)	Ba_2CeNbO_6: Eu^{3+} (2.5%)
Structure		Monoclinic	Monoclinic	Monoclinic	Monoclinic	Monoclinic	Monoclinic
Space Group		$P2_1/n$	$P2_1/n$	$P2_1/n$	$P2_1/n$	$P2_1/n$	$P2_1/n$
Cell Parameters	**a(Å)**	5.9012(2)	5.9115(5)	5.9052(7)	5.9168(4)	5.9132(3)	5.9048(5)
	b(Å)	6.1043(8)	6.0854(3)	6.0986(9)	6.0943(5)	6.1013(7)	6.0972(8)
	c(Å)	8.0586(3)	8.0795(2)	8.0626(3)	8.0746(6)	8.0816(8)	8.0716(4)
	β	90.06	90.05	89.96	89.93	90.12	89.98
Volume $(Å)^3$		290.29	290.65	290.36	291.16	291.56	290.59
Average Crystallite Size (nm)	**Scherrer Method**	24.1	25.4	20.8	21.1	22.1	19.8
	W-H Plot	23.8	25.9	21.3	20.9	21.6	20.1
Strain (ε)		4.33×10^{-3}	4.96×10^{-3}	2.14×10^{-3}	1.41×10^{-3}	2.49×10^{-3}	1.49×10^{-3}

Table 5.3 Summary of cell parameter, volume and crystalline size of Eu(III) doped Ba_2CeNbO_6.

5.3.2 FTIR (Fourier Transform Infrared Spectrometry)

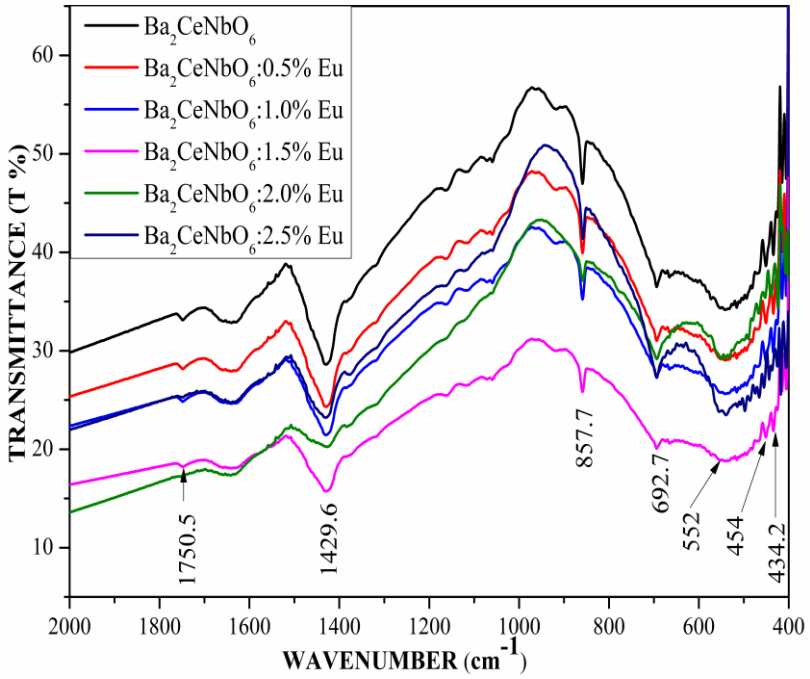

Figure 5.3 FTIR spectra of undoped and Eu(III) doped Ba_2CeNbO_6.

To discover the atomic bonds in a compound FTIR analysis has been carried out. In Figure 5.3 FTIR spectra of Ba_2CeNbO_6 has shown with a range of 400 cm^{-1} to 2000 cm^{-1} wavenumber. The FTIR spectrum of Ba_2CeNbO_6 shows some well-defined bands in the above figure. It is in good accordance with group theory predictions what orderly found for pervoskite type structures [42]. In pervoskite-type material, significant vibrational couplings may expect between the different coordination polyhedral compounds. All the peaks in the spectra are typical of the material. One small hump is at 1750 cm^{-1}, which is due to the presence of adsorbed moisture in KBr [43]. The lower energy band found at around 450–650 cm^{-1} is related to the deformational mode of CeO_6 octahedra [44]. The medium energy peak appearing near 850 cm^{-1} is due to the asymmetric NbO_6 stretching vibration [45] due to the higher charge of the cation. The strong intensity peak at approximately 1430 cm^{-1} can eventually be related to the symmetric stretching vibration of NbO_6 octahedra [46]. A small intensity peak at 1100 cm^{-1} likely corresponds to the presence of overtones of the fundamental vibrations in Ba_2CeNbO_6 [47]. The peak at 552cm^{-1} is due to the Ba-O.

5.3.3 Photoluminescence

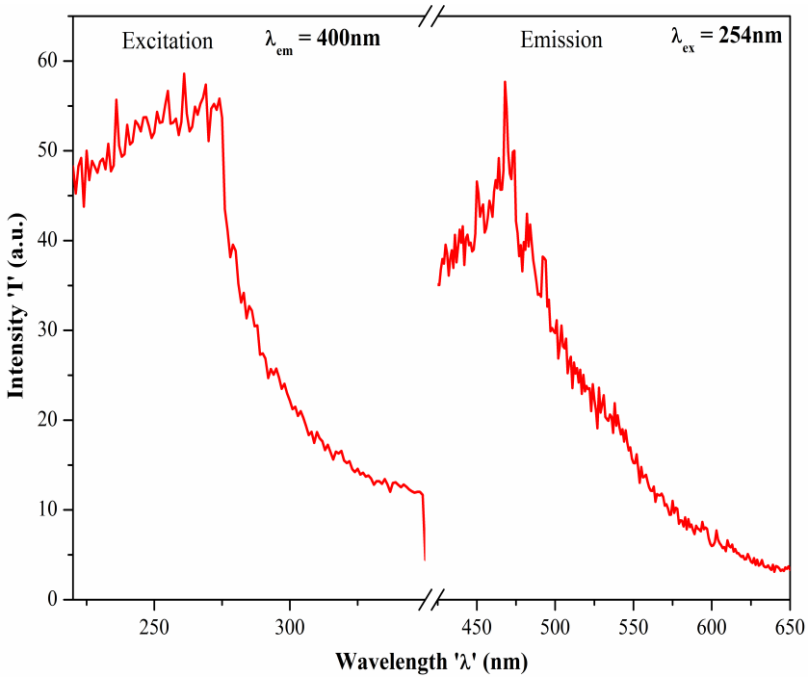

Figure 5.4 Photoluminescence spectra of Ba_2CeNbO_6.

Figure 5.4 shows room temperature excitation and emission spectra of undoped Ba_2CeNbO_6. Emission spectra of undoped Ba_2CeNbO_6 phosphor were recorded by exciting this phosphor with 254nm wavelength and excitation spectra recorded with 400nm emission wavelength.

Figure 5.5 represents the absorption spectra of Eu(III) doped Ba_2CeNbO_6 phosphor. These excitation spectra recorded with the 613nm emission wavelength. An intense peak at 466 nm wavelength is due to the $^5D_2 \leftarrow {}^7F_0$ electric dipole transition [48]. The absorption spectra are less used and their analysis is also less useful. The main reason for this is that the most relevant transitions for the determination of the point group symmetry ($^5D_0 \leftarrow {}^7F_0$, $^5D_1 \leftarrow {}^7F_1$, $^5D_1 \leftarrow {}^7F_0$, $^5D_2 \leftarrow {}^7F_1$, and $^5D_2 \leftarrow {}^7F_0$) are very weak. The absorption spectra of Eu(III) compounds allows the determination of higher energy levels of the $^4f_6$ electronic configuration of Eu^{3+} ion. In the earlier literature survey, the transitions to the $^5D_0$, $^5D_1$, and $^5D_2$ levels were called the yellow, green and blue bands based on their places in the visible spectrum [49, 50]. The transitions of $^5D_0 \leftarrow {}^7F_1$ and $^5D_0 \leftarrow {}^7F_2$ are suitable for determining the location of the $^5D_0$ level if the $^5D_0 \leftarrow {}^7F_0$ transition is forbidden.

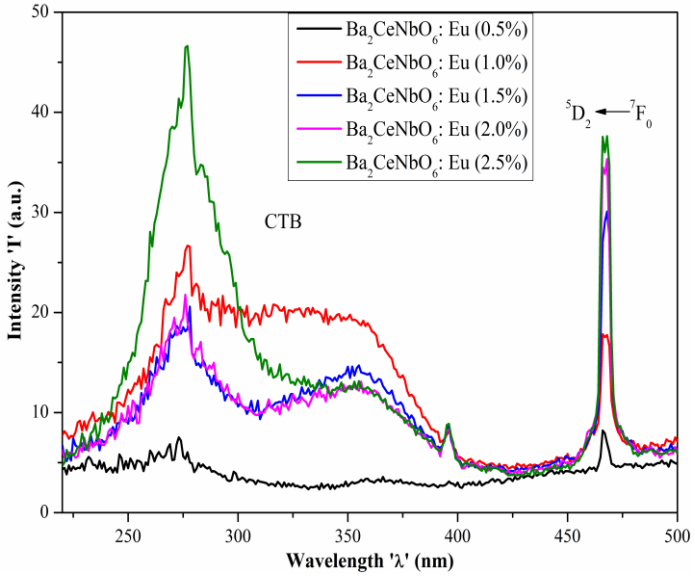

Figure 5.5 Photoluminescence Excitation spectra of Eu(III) doped Ba_2CeNbO_6.

For transitions to the $^5D_2$ level, the $^5D_2 \leftarrow ^7F_0$ transition is the most useful, because it allows determining the location of the $^5D_2$ level. This $^5D_2 \leftarrow ^7F_0$ electric dipole transition is hypersensitive ($\Delta J = 2$). The hypersensitivity of the $^5D_2 \leftarrow ^7F_0$ transition is very well explained by examining the europium(III) dipicolinate system [51]. The $^5D_2$ level is often used to directly excite the Eu^{3+} ion with one of the lines of an argon-ion laser (465.8 nm) or with a diode laser.

Europium (III) also shows broad absorption bands in the UV region of the electromagnetic spectrum. This broad absorption band is due to an electron transfer from one or more adjacent atoms to the Eu^{3+} ion. Eu^{3+} is the most oxidizing ion of the trivalent rare-earth ions as Eu^{3+} is requiring only a single electron to achieve a half-filled stable shell. These absorption bands in the UV region are so-called charge-transfer (CT) bands or ligand-to-metal charge transfer (LMCT) bands. These absorption bands are very intense related to the f–f transitions as these transitions are allowed by the Laporte selection rule [52]. The location of charge-transfer bands strongly depending on the nature of the ligands. The relationship between the nature of the ligands and the position of the charge-transfer bands was first recognized by Ryan and Jørgensen [53] but, it was studied by Dorenbos [54, 55] in more detail. Dorenbos gives an extensive compilation of the energies of the charge-transfer transitions of Eu(III) compounds in the solid state [55]. The general trend of the energies of the charge-transfer transitions is: fluorides > oxides > nitrides > chlorides > bromides > iodides > sulfides >selenides > phosphides > arsenides > tellurides > antimonides [48].

Charge-transfer states of Eu^{3+} at low energies possess severe consequences for the spectroscopic characteristics of Eu^{3+} ion, due to the non-negligible mixing of the $^4f_6$ electronic states and the charge-transfer states. This mixing has been utilized to explain the high intensity of the $^5D_0 \rightarrow {}^7F_0$ transition in some europium(III) compounds [56]. Charge-transfer bands also useful for the sensitization of europium(III) luminescence as they can work as aerial to consume energy and transfer this excitation energy to the Eu^{3+} ion.

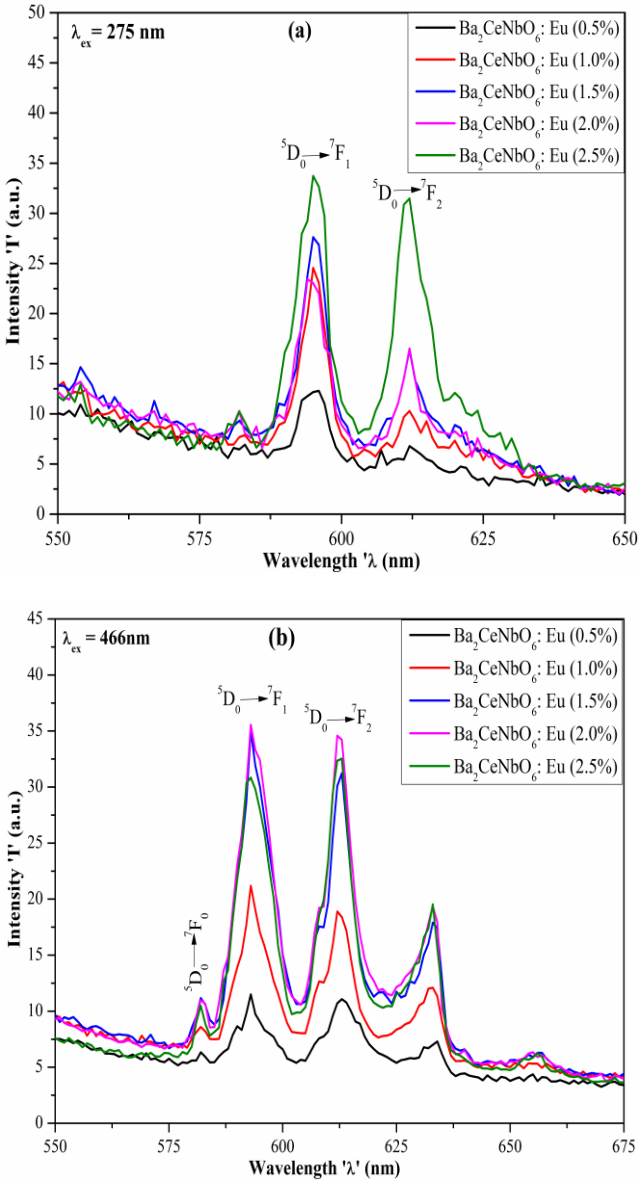

Figure 5.6 Photoluminescence emission spectra of Eu(III) doped Ba_2CeNbO_6 (a) excitation wavelength 275nm and (b) excitation wavelength 466nm.

Fig. 5.6 (a) and (b) depict typical PL emission spectra of Eu (III) doped Ba_2CeNbO_6 phosphors excited with 275nm and 466nm wavelength. In the present study, the concentration of europium ranges from 0.5 to 2.5 mole percentage. The Eu (III) doped Ba_2CeNbO_6 phosphors exhibit two visible emission bands around 596 and 613 nm when excited at 275nm while it displays four emission peaks at 582nm, 596nm, 613nm, and 633nm. These emission peaks are assigned to the magnetic dipole (MD) $^5D_0 \rightarrow {}^7F_1$ and electric dipole (ED) $^5D_0 \rightarrow {}^7F_2$ transitions of europium when excited with 275nm and 466nm. The emission peak at 596 nm is due to the magnetic dipole transition of $^5D_0 \rightarrow {}^7F_1$, which has higher intensity compare to peak at 613nm of $^5D_0 \rightarrow {}^7F_2$ electric dipole transition during excitation at 275nm. This asymmetricity confirms that the Eu^{3+} ions are located at the non-inversion symmetric sites in host material [57 – 59]. When this phosphor was excited at 466nm emission peaks are observed at around 580-600 nm, this is mainly due to the magnetic dipole transition of $^5D_0 \rightarrow {}^7F_0$ and $^5D_0 \rightarrow {}^7F_1$ and emission peak at 613nm and 633nm are due to electric dipole transition of the $^5D_0 \rightarrow {}^7F_2$**.**

It's important to note that in both the emission spectra emission peak at around 613nm is occurred in the red region. In emission spectra peak at 633nm seen when phosphor excited at 466nm wavelength, which is attributed due to $^5D_0 \rightarrow {}^7F_2$ electric dipole transition. Though an admixture of odd-parity electronic configuration to the pure 4f (like a non-centrosymmetric crystal field component) [60, 61] will allow the ED transitions partially and their possibility of occurrence is much higher than the probability of parity-allowed magnetic dipole (MD) ($^5D_0 \rightarrow {}^7F_1$) transition. The site symmetry of Eu^{3+} ion in the host lattice can be predicted by asymmetry ratio, which can be defined as equation (5.4),

$$asymmetry - ratio = \frac{I(5D_0 \rightarrow 7F_2)}{I(5D_0 \rightarrow 7F_1)} \text{ ---------- (5.4)}$$

Where, I ($^5D_0 \rightarrow {}^7F_2$) and I ($^5D_0 \rightarrow {}^7F_1$) are the intensities of electric dipole and magnetic dipole transitions respectively. When asymmetry ratio > 1, then Eu (III) substituted at the non-centrosymmetric site, and the asymmetry ratio < 1 then Eu(III) substituted at a centrosymmetric site in the host lattice. Table 5.4 shows the asymmetry ratio for both emission spectra. In the present research, the asymmetric ratio is found to be less than unity (1), indicates that Eu (III) is substituted at a non-centrosymmetric site in the host lattice, and it's in good agreement with the earlier report [59, 62 – 66]. It saw

that the substitution of Eu (III) at the place of Ba (II) site in Ba_2CeNbO_6 is followed by Ba(II) ion vacancy due to a distinct ionic radius. These gaps in lattice reduce the local site symmetry at the Eu(III) site and act as a luminescence quenching center.

Sample	Asymmetry Ratio	
	at 275nm	at 466nm
Ba_2CeNbO_6:Eu (0.5%)	0.550	0.974
Ba_2CeNbO_6:Eu (1.0%)	0.419	0.896
Ba_2CeNbO_6:Eu (1.5%)	0.597	0.908
Ba_2CeNbO_6:Eu (2.0%)	0.704	0.978
Ba_2CeNbO_6:Eu (2.5%)	0.933	1.055

Table 5.4 Asymmetric ratio of Eu(III) doped Ba_2CeNbO_6 at 275nm and 466nm emission spectra.

The results presented in Fig. 5.6 (a & b) reveal that the spectral profile of the phosphors show noticeable changes with increasing europium concentration and the mixed overall emission light chromaticity.

CIE (Commission International del'éclairage)

The chromaticity color coordinates of all phosphors were determined, and the results are presented in the Commission International del'éclairage (CIE) 1931 diagram, as shown in Figure 5.7 (a) and (b). With increasing europium (III) concentration, the color tone of the emanating light shifts from the orange region to the red region [65, 67 – 69]. It's good to point out that the continuity of the emission tone corresponding to coordinate points shown in Figure 5.7 by exciting the sample at 275nm and 466nm wavelength. This allows a mixture of light with color in the white-light region supports the intense glow correlated color temperature, i.e., CCT in the 1800–5000K temperature range. We have indeed simulated the generation flow CCT white-light using xenon lamp of the phosphors reported here and the CIE1931 coordinates, and associated correlated color temperature (CCT) of the all phosphors presented in Table 5.5.

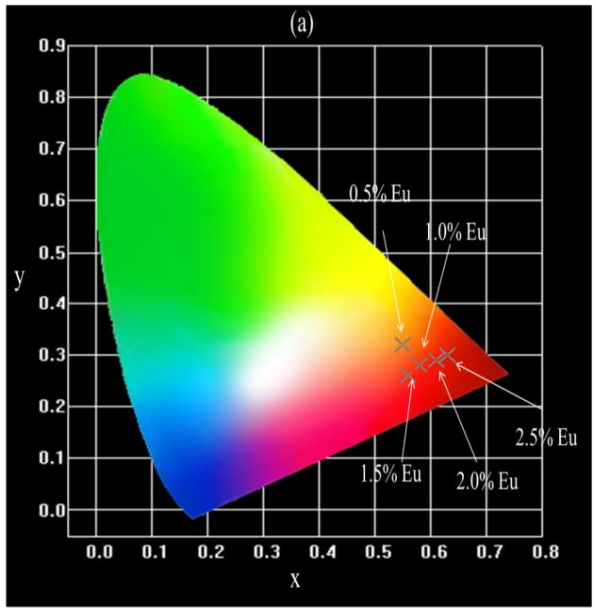

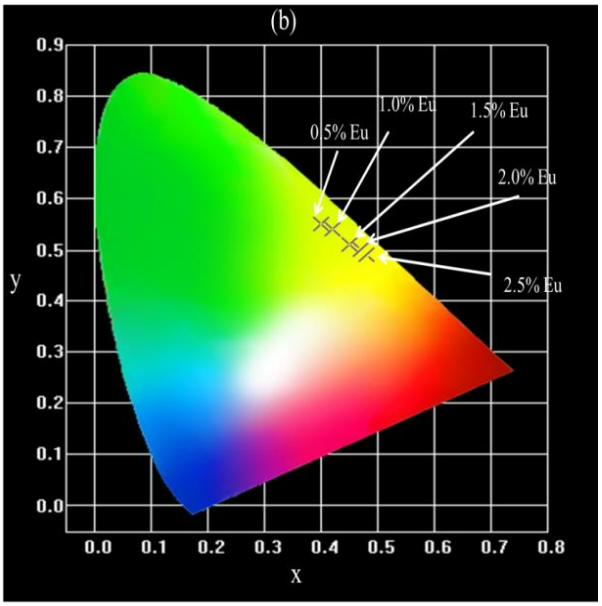

Figure 5.7 CIE diagram of Eu(III) doped Ba_2CeNbO_6 (a) emission at 275nm (b) emission at 466nm.

Sr. No.	Sample	275nm				466nm			
		x	y	CCT		x	y	CCT	
				Calcu.	Software			Calculated	Software
1	Ba_2CeNbO_6:Eu (0.5%)	0.55	0.32	1813.4	1825	0.40	0.55	4366.3	4359
2	Ba_2CeNbO_6:Eu (1.0%)	0.58	0.28	3795.6	3798	0.42	0.54	4035.8	4028
3	Ba_2CeNbO_6:Eu (1.5%)	0.56	0.26	4809.9	4813	0.45	0.51	3482.2	3476
4	Ba_2CeNbO_6:Eu (2.0%)	0.61	0.29	3880.2	3878	0.47	0.50	3165.4	3161
5	Ba_2CeNbO_6:Eu (2.5%)	0.63	0.30	3739.8	3742	0.48	0.49	2983.3	2981

Table 5.5 CIE 1931 coordinates and CCT of the emissions under (275nm and 466nm) xenon lamp excitation.

5.4 Outcome

Eu^{3+} doped Barium Cerium Niobate (BCN) oxide has been synthesizing by the combustion synthesis method. The X-ray diffraction measurement of Barium Cerium Niobate (BCN) oxide revels that phosphor has a monoclinic phase with space group $P2_1/n$ (# 014). Prepared pervoskite phosphor is nanocrystalline measured through Scherrer's method and Williamson-hall plot method. Angle Shift in XRD patterns is also reflected in the Williamson–Hall plot, which occurred due to the highly strained and distorted environment in the Ba_2CeNbO_6 lattice**.**

FTIR of Ba_2CeNbO_6 gives information that phosphor has a nano-size pervoskite structure with an edge-connected Nb-O octahedral. The peak at $552cm^{-1}$ is due to the Ba-O. One small hump is at 1750 cm^{-1}, which is due to the presence of adsorbed moisture in KBr. The lower energy band found at around 450–650 cm^{-1} is related to the deformational mode of CeO_6 octahedra. A small intensity peak at 1100 cm^{-1} likely corresponds to the presence of overtones of the fundamental vibrations in Ba_2CeNbO_6.

Room temperature photoluminescence spectra of phosphor recorded using a Xenon lamp as a source. A Photoluminescence study of Eu^{3+} doped Ba_2CeNbO_6 phosphor shows Eu (III) is substituted at a non-centrosymmetric site in the host lattice for 275nm and 466nm. Photoluminescence spectra of phosphor show high-intensity peaks at 590nm and 613nm due to $^5D_0 \rightarrow {}^7F_1$ and $^5D_0 \rightarrow {}^7F_2$ transitions of Eu^{3+} ions. The peak at 623nm is maybe due to electronic transition ($^5D_0 \rightarrow {}^7F_2$) of Eu^{3+}.The substitution of Eu^{3+} at Ba^{2+} site in Ba_2CeNbO_6 is followed by Ba^{2+} ion vacancy due to charge imbalance and lattice strain due to different ionic radius. With the increasing europium concentration, the colour tone of the emanating light shifts from orange to the red region. The emission colour corresponding to coordinate points yields a mixture of light with colour in the orange-red region possess glow correlated colour temperature, i.e., CCT in the 1800K – 5000K range.

References

[1] S. K. Korchagina, N. V. Golubko, Y. A. Shevchuk, and V. V. Gagulin, "Dilatometry and Dielectric Properties of Ba 2 RTaO 6 (R = La, Pr, Sm, Dy) Ceramics," *Inorg. Mater.*, vol. 40, no. 10, pp. 1088–1090, Oct. 2004.

[2] S. K. Korchagina and Y. A. Shevchuk, "Low-frequency and microwave dielectric properties of Ba2LnTaO6 (Ln = La, Pr, Sm, Dy, Ce, Gd, Nd, Tm, Tb) ceramics," *Inorg. Mater.*, vol. 42, no. 1, pp. 64–67, Jan. 2006.

[3] T. G. N. Babu and J. Koshy, "Ba2RETaO6(RE= Pr, Nd, Eu, and Dy), A Group of Chemically Stable Substrates for YBa2Cu3O7−δFilms," *J. Solid State Chem.*, vol. 126, no. 2, pp. 202–207, Nov. 1996.

[4] J. Kurian, J. Koshy, P. R. S. Wariar, Y. P. Yadava, and A. D. Damodaran, "Synthesis and Characterization of Rare-Earth Barium Antimonates, a New Group of Complex Pervoskites Suitable as Substrates for YBa2Cu3O7-δ Films," *J. Solid State Chem.*, vol. 116, no. 1, pp. 193–198, Apr. 1995.

[5] J. Kurian, A. M. John, P. K. Sajith, J. Koshy, S. P. Pai, and R. Pinto, "Growth of YBCO–Ag thin films (Tc(0)=90 K) by pulsed laser ablation on polycrystalline Ba2EuNbO6; A new pervoskite ceramic substrate for YBCO films," *Mater. Lett.*, vol. 34, no. 3–6, pp. 208–212, Mar. 1998.

[6] E. J. Cussen, D. R. Lynham, and J. Rogers, "Magnetic Order Arising from Structural Distortion: Structure and Magnetic Properties of Ba 2 LnMoO 6," *Chem. Mater.*, vol. 18, no. 12, pp. 2855–2866, Jun. 2006.

[7] W. T. A. Harrison, K. P. Reis, A. J. Jacobson, L. F. Schneemeyer, and J. V. Waszczak, "Syntheses, Structures, and Magnetism of Barium/Rare-Earth/Bismuth Double Pervoskites. Crystal Structures of Ba2MBiO6 (M = Ce, Pr, Nd, Tb, Yb) by Powder Neutron Diffraction," *Chem. Mater.*, vol. 7, no. 11, pp. 2161–2167, Nov. 1995.

[8] Y. Doi and Y. Hinatsu, "Magnetic properties of ordered pervoskites Ba 2 LnTaO 6 (Ln = Y, lanthanides)," *J. Phys. Condens. Matter*, vol. 13, no. 19, pp. 4191–4202, May 2001.

[9] K. Henmi, Y. Hinatsu, and N. M. Masaki, "Crystal Structures and Magnetic Properties of Ordered Pervoskites Ba2LnNbO6 (Ln=Lanthanide Elements)," *J. Solid State Chem.*, vol. 148, no. 2, pp. 353–360, Dec. 1999.

[10] Y. Hinatsu *et al.*, "Studies on magnetic and calorimetric properties of double pervoskites Ba2HoRuO6 and Ba2HoIrO6," *J. Solid State Chem.*, vol. 177, no. 1, pp. 38–44, Jan. 2004.

[11] C. C. Yu *et al.*, "Enhanced photoluminescence of Ba2GdNbO6: Eu3+/Dy3+ phosphors by Li+ doping," *J. Solid State Chem.*, vol. 180, no. 11, pp. 3058–3065, Nov. 2007.

[12] G. King and P. M. Woodward, "Cation ordering in pervoskites," *J. Mater. Chem.*, vol. 20, no. 28, p. 5785, 2010.

[13] E. A. R. Assirey, "Pervoskite synthesis, properties and their related biochemical and industrial application," *Saudi Pharm. J.*, vol. 27, no. 6, pp. 817–829, Sep. 2019.

[14] J. Liang *et al.*, "An all-inorganic pervoskite solar capacitor for efficient and stable spontaneous photocharging," *Nano Energy*, vol. 52, pp. 239–245, Oct. 2018.

[15] R. Chen *et al.*, "Transient Resistive Switching for Nonvolatile Memory Based on Water-Soluble Cs 4 PbBr 6 Pervoskite Films," *Phys. status solidi – Rapid Res. Lett.*, vol. 13, no. 11, p. 1900397, Nov. 2019.

[16] D. Liu *et al.*, "Flexible All-Inorganic Pervoskite CsPbBr 3 Nonvolatile Memory Device," *ACS Appl. Mater. Interfaces*, vol. 9, no. 7, pp. 6171–6176, Feb. 2017.

[17] N. T. Thuy, D. Le Minh, H. T. Giang, and N. N. Toan, "Structural, Electrical, and Ethanol-Sensing Properties of La1-xNdxFeO3 Nanoparticles," *Adv. Mater. Sci. Eng.*, vol. 2014, pp. 1–5, 2014.

[18] F. Li *et al.*, "Piezoelectric activity in Pervoskite ferroelectric crystals," *IEEE Trans. Ultrason. Ferroelectr. Freq. Control*, vol. 62, no. 1, pp. 18–32, Jan. 2015.

[19] S. B. Karki, R. K. Hona, and F. Ramezanipour, "Effect of Structure on Sensor Properties of Oxygen-Deficient Pervoskites, A2BB′O5 (A = Ca, Sr; B = Fe; B′ = Fe, Mn) for Oxygen, Carbon Dioxide and Carbon Monoxide Sensing," *J. Electron. Mater.*, vol. 49, no. 2, pp. 1557–1567, Feb. 2020.

[20] Y. Bai, T. Siponkoski, J. Peräntie, H. Jantunen, and J. Juuti, "Ferroelectric, pyroelectric, and piezoelectric properties of a photovoltaic pervoskite oxide," *Appl. Phys. Lett.*, vol. 110, no. 6, p. 063903, Feb. 2017.

[21] J.-C. Liu, Y.-T. Cheng, S.-Y. Ho, H.-S. Hung, and S.-H. Chang, "Fabrication and Characterization of High-Sensitivity Underwater Acoustic Multimedia

Communication Devices with Thick Composite PZT Films," *J. Sensors*, vol. 2017, pp. 1–7, 2017.

[22] I. Dursun *et al.*, "Pervoskite Nanocrystals as a Color Converter for Visible Light Communication," *ACS Photonics*, vol. 3, no. 7, pp. 1150–1156, Jul. 2016.

[23] L. Chouhan, S. Ghimire, C. Subrahmanyam, T. Miyasaka, and V. Biju, "Synthesis, optoelectronic properties and applications of halide pervoskites," *Chem. Soc. Rev.*, 2020.

[24] L. Brixner, "Preparation and crystallographic study of some new rare earth compounds," *J. Inorg. Nucl. Chem.*, vol. 15, no. 3–4, pp. 352–355, Oct. 1960.

[25] M. Takata and K. Kageyama, "Microwave Characteristics of A(B3+1/2B5+1/2)O3 Ceramics (A = Ba, Ca, Sr; B3+ = La, Nd, Sm, Yb; B5+ = Nb, Ta)," *J. Am. Ceram. Soc.*, vol. 72, no. 10, pp. 1955–1959, Oct. 1989.

[26] F. V. S and F. E. G, "Preparation and Unit-Cell Parameters of Ä2ÇIBIIO6 Compounds," *Kristallografiya*, vol. 6, no. 5, pp. 770–772, 1961.

[27] M. ANDERSON, K. GREENWOOD, G. TAYLOR, and K. POEPPELMEIER, "B-cation arrangements in double pervoskites," *Prog. Solid State Chem.*, vol. 22, no. 3, pp. 197–233, 1993.

[28] U. Amador, C. J. D. Hetherington, E. Moran, and M. A. Alario-Franco, "Ba2PrPtO6: A novel double pervoskite," *J. Solid State Chem.*, vol. 96, no. 1, pp. 132–140, Jan. 1992.

[29] G. Blasse, "New compounds with pervoskite-like structures," *J. Inorg. Nucl. Chem.*, vol. 27, no. 5, pp. 993–1003, May 1965.

[30] M. P. Attfield, P. D. Battle, S. K. Bollen, T. C. Gibb, and R. J. Whitehead, "The crystal structure and magnetic properties of SrLaFeSnO6 and SrLaNiSbO6," *J. Solid State Chem.*, vol. 100, no. 1, pp. 37–48, Sep. 1992.

[31] P. D. Battle, J. B. Goodenough, and R. Price, "The crystal structures and magnetic properties of Ba2LaRuO6 and Ca2LaRuO6," *J. Solid State Chem.*, vol. 46, no. 2, pp. 234–244, Feb. 1983.

[32] R. ROY, "Multiple Ion Substitution in the Pervoskite Lattice," *J. Am. Ceram. Soc.*, vol. 37, no. 12, pp. 581–588, Dec. 1954.

[33] M. P. Attfield, P. D. Battle, S. K. Bollen, S. H. Kim, A. V. Powell, and M. Workman, "Structural and electrical studies of mixed copper/ruthenium oxides

and related compounds of zinc and antimony," *J. Solid State Chem.*, vol. 96, no. 2, pp. 344–359, Feb. 1992.

[34] M. T. Anderson and K. R. Poeppelmeier, "Lanthanum copper tin oxide (La2CuSnO6): a new pervoskite-related compound with an unusual arrangement of B cations," *Chem. Mater.*, vol. 3, no. 3, pp. 476–482, May 1991.

[35] M. Srinivas, V. Verma, N. Patel, D. Modi, D. Tawde, and K. V. R. Murthy, "Characterization of newly synthesized Strontium Cerium Niobate nanophosphor," *J. Lumin.*, vol. 147, pp. 324–327, Mar. 2014.

[36] A. Dutta and T. P. Sinha, "Dielectric Relaxation and Electronic Structure of Double Pervoskite Ca2AlNbO6," *Integr. Ferroelectr.*, vol. 116, no. July 2015, pp. 41–50, 2010.

[37] L. A. Khalam and M. T. Sebastian, "Effect of Cation Substitution and Non-Stoichiometry on the Microwave Dielectric Properties of Sr(B' 0.5 Ta 0.5)O 3 [B'=Lanthanides] Pervoskites," *J. Am. Ceram. Soc.*, vol. 89, no. 12, pp. 3689–3695, Dec. 2006.

[38] C. Suryanarayana and M. G. Norton, *X-Ray Diffraction*, 1st ed. Boston, MA: Springer US, 1998.

[39] V. M. Goldschmidt, "Die Gesetze der Krystallochemie," *Naturwissenschaften*, vol. 14, no. 21, pp. 477–485, 1926.

[40] R. D. Shannon, "Revised effective ionic radii and systematic studies of interatomic distances in halides and chalcogenides," *Acta Crystallogr. Sect. A*, vol. 32, no. 5, pp. 751–767, Sep. 1976.

[41] M. W. Lufaso and P. M. Woodward, "Prediction of the crystal structures of pervoskites using the software program SPuDS," *Acta Crystallogr. Sect. B*, vol. 57, no. 6, pp. 725–738, 2001.

[42] M. Licheron, F. Gervais, J. Coutures, and J. Choisnet, "'Ba2BiO4' surprisingly found as a cubic double pervoskite," *Solid State Commun.*, vol. 75, no. 9, pp. 759–763, Sep. 1990.

[43] J. E. Yoo and J. Choi, "Surfactant-assisted growth of anodic nanoporous niobium oxide with a grained surface," *Electrochim. Acta*, vol. 55, no. 18, pp. 5142–5147, Jul. 2010.

[44] Y. Huang, T. Wei, and Y. Ge, "Preparation and characterization of novel Ce(III)-

gelatin complex," *J. Appl. Polym. Sci.*, vol. 108, no. 6, pp. 3804–3807, Jun. 2008.

[45] J. LIN *et al.*, "Crystallization of TeO2–Nb2O5 glasses and their network structural evolution," *Mater. Sci.*, vol. 27, p. 329, 2009.

[46] X. Jin, D. Sun, M. Zhang, Y. Zhu, and J. Qian, "Investigation on FTIR spectra of barium calcium titanate ceramics," *J. Electroceramics*, vol. 22, no. 1–3, pp. 285–290, Feb. 2009.

[47] A. E. Lavat, M. C. Grasselli, E. J. Baran, and R. C. Mercader, "Spectroscopic characterization of Ba LnSnO materials: 2 5.5 ceramic substrates for high T superconductors," *Mater. Latters*, vol. 47, no. 4–5, pp. 194–198, 2001.

[48] K. Binnemans, "Interpretation of europium(III) spectra," *Coord. Chem. Rev.*, vol. 295, pp. 1–45, Jul. 2015.

[49] K. H. Hellwege and H. G. Kahle, "Spektrum und Struktur kristalliner Europiumsalze. I. Europiumchlorid EuCI2. 6 H2O.," *Zeitschrift f*[illegible]*r Phys.*, vol. 129, no. 1, pp. 62–84, Jan. 1951.

[50] K. H. Hellwege and H. G. Kahle, "Spectrum and structure of crystalline europium salts II. Europiumbromat Eu (BrO 3) 3 · 9H 2 O," *Zeitschrift f*[illegible]*r Phys.*, vol. 129, no. 1, pp. 85–103, Jan. 1951.

[51] K. Binnemans, K. Van Herck, and C. Görller-Walrand, "Influence of dipicolinate ligands on the spectroscopic properties of europium(III) in solution," *Chem. Phys. Lett.*, vol. 266, no. 3–4, pp. 297–302, Feb. 1997.

[52] O. Laporte and W. F. Meggers, "Some Rules of Spectral Structure*," *J. Opt. Soc. Am.*, vol. 11, no. 5, p. 459, Nov. 1925.

[53] P. Dorenbos, "5d -level energies of Ce3+ and the crystalline environment. I. Fluoride compounds," *Phys. Rev. B*, vol. 62, no. 23, pp. 15640–15649, Dec. 2000.

[54] P. Dorenbos, "Systematic behaviour in trivalent lanthanide charge transfer energies," *J. Phys. Condens. Matter*, vol. 15, no. 49, pp. 8417–8434, Dec. 2003.

[55] P. Dorenbos, "The Eu3+ charge transfer energy andthe relation with the band gap of compounds," *J. Lumin.*, vol. 111, no. 1–2, pp. 89–104, Jan. 2005.

[56] X. Y. Chen and G. K. Liu, "The standard and anomalous crystal-field spectra of Eu3+," *J. Solid State Chem.*, vol. 178, no. 2, pp. 419–428, Feb. 2005.

[57] R. Rajaramakrishna, P. Nijapai, P. Kidkhunthod, H. J. Kim, J. Kaewkhao, and Y. Ruangtaweep, "Molecular dynamics simulation and luminescence properties of

Eu3+ doped molybdenum gadolinium borate glasses for red emission," *J. Alloys Compd.*, vol. 813, p. 151914, Jan. 2020.

[58] S. Som, A. Choubey, and S. K. Sharma, "Spectral and trapping parameters of Eu 3+ in Gd 2 O 2 S nanophosphor," *J. Exp. Nanosci.*, vol. 10, no. 5, pp. 350–370, Mar. 2015.

[59] N. Pathak, S. Mukherjee, D. Das, D. Dutta, S. Dash, and R. M. Kadam, "Evolution of different defect clusters in Eu 3+ doped KMgF 3 and Eu 3+ , Li + co-doped KMgF 3 compounds and the immediate impact on the phosphor characteristics," *J. Mater. Chem. C*, 2020.

[60] Y. Shimada, H. Kiyama, and Y. Tokura, "Magnetoelectric emission in rare-earth doped ferroelectric crystals La2Ti2O7 :R3+ (R=Er, Eu, and Nd)," *Phys. Rev. B*, vol. 75, no. 24, p. 245125, Jun. 2007.

[61] G. B. F. Bosco and L. R. Tessler, "Crystal field parameters of the C2 site in Eu2O3," *Opt. Mater. X*, vol. 2, p. 100028, May 2019.

[62] X. Zhao *et al.*, "Efficient red phosphor double-pervoskite Ca3WO6 with A-site substitution of Eu3+," *Dalt. Trans.*, vol. 42, no. 37, p. 13502, 2013.

[63] X. Zhao, Y. Ding, Z. Li, T. Yu, and Z. Zou, "An efficient charge compensated red phosphor Sr3WO6: K+, Eu3+ – For white LEDs," *J. Alloys Compd.*, vol. 553, pp. 221–224, Mar. 2013.

[64] S. Zhang, Y. Hu, L. Chen, X. Wang, G. Ju, and Y. Fan, "Photoluminescence properties of Ca3WO6:Eu3+ red phosphor," *J. Lumin.*, vol. 142, pp. 116–121, Oct. 2013.

[65] K. V. Dabre, K. Park, and S. J. Dhoble, "Synthesis and photoluminescence properties of microcrystalline Sr 2 ZnWO 6 :RE 3+ (RE = Eu, Dy, Sm and Pr) phosphors," *J. Alloys Compd.*, vol. 617, pp. 129–134, Dec. 2014.

[66] A. Fu *et al.*, "A novel double pervoskite La2ZnTiO6:Eu3+ red phosphor for solid-state lighting: Synthesis and optimum luminescence," *Opt. Laser Technol.*, vol. 96, pp. 43–49, Nov. 2017.

[67] Y. Zhang, J. Xu, Q. Cui, and B. Yang, "Eu3+-doped Bi4Si3O12 red phosphor for solid state lighting: microwave synthesis, characterization, photoluminescence properties and thermal quenching mechanisms," *Sci. Rep.*, vol. 7, no. 1, p. 42464, Mar. 2017.

[68] Y. Gao *et al.*, “Tb 3+ and Eu 3+ co-doped Ba 6 Bi 9 B 79 O 138 : color-tunable phosphors by utilizing the host-sensitization effect of Bi 3+ and enhancement of red emission upon heating,” *New J. Chem.*, vol. 41, no. 5, pp. 2037–2045, 2017.

[69] A. Katelnikovas, H. Winkler, A. Kareiva, and T. Jüstel, “Synthesis and optical properties of green to orange tunable garnet phosphors for pcLEDs,” *Opt. Mater. (Amst).*, vol. 33, no. 7, pp. 992–995, May 2011.